Journal of
Synchrotron
Radiation

ISSN 0909-0495

Received 29 May 2012
Accepted 8 October 2012

Local and electronic structure around Ga in CdTe: evidence of DX- and A-centers

Vasil Koteski,[a,b]* Jelena Belošević-Čavor,[a] Petro Fochuk[c] and Heinz-Eberhard Mahnke[b,d]

[a]Vinča Institute of Nuclear Sciences, University of Belgrade, Belgrade, Serbia, [b]Helmholtz-Zentrum Berlin für Materialien und Energie GmbH, Berlin, Germany, [c]Chernivtsi National University, Chernivtsi, Ukraine, and [d]Freie Universität Berlin, Fachbereich Physik, Berlin, Germany. E-mail: vkotes@vin.bg.ac.rs

The lattice relaxation around Ga in CdTe is investigated by means of extended X-ray absorption spectroscopy (EXAFS) and density functional theory (DFT) calculations using the linear augmented plane waves plus local orbitals (LAPW + lo) method. In addition to the substitutional position, the calculations are performed for DX- and A-centers of Ga in CdTe. The results of the calculations are in good agreement with the experimental data, as obtained from EXAFS and X-ray absorption near-edge structure (XANES). They allow the experimental identification of several defect structures in CdTe. In particular, direct experimental evidence for the existence of DX-centers in CdTe is provided, and for the first time the local bond lengths of this defect are measured directly.

Keywords: lattice relaxation; augmented plane waves plus local orbitals; defect structures.

1. Introduction

CdTe has been researched extensively in the past owing to its interesting applications in optoelectronics. Various dopants are often introduced in CdTe in order to improve its optical and electrical properties. While the interest in CdTe used to be wide with respect to opto-electronic applications, with the characteristics of the basic material summarized by Rössler (1999), most recently the interest in CdTe has risen rather rapidly because of its high detection efficiency for X- and γ-radiation for astronomy and medical imaging detectors (Del Sordo *et al.*, 2009). Therefore, basic research for improving the preparation and processing of the basic material as well as the fabrication of thin film or nano-structures is receiving continuing attention (for example, see the monograph by Triboulet & Siffert, 2010). For optimal performance the incorporation of defects influencing the electrical behavior, *e.g.* the trapping of charge carriers, must be controlled and understood. The introduction of impurities in CdTe is in many cases followed by lattice distortions and the formation of defect complexes, which in turn influence the electronic features of the system (Koteski *et al.*, 2005; Mahnke *et al.*, 2005). Ga and In are highly soluble dopants in CdTe and this allows their solid solutions to be obtained up to a concentration of 10^{20} atoms cm^{-3} (Panchuk & Fochuk, 2010). The properties of CdTe:In crystals are well studied as published in various articles; however, gallium point-defect structures have been investigated much less, especially at the high-temperature point-defect equilibrium (Fochuk *et al.*, 2002, 2004). In highly doped CdTe:Ga, besides the substitutional Ga_{Cd} position, Ga is primarily expected to form an A-center (complex with a nearby cation vacancy) and a DX-center (Chadi & Chang, 1988; Park & Chadi, 1995) (accompanied by significant lattice relaxation around the dopant). In addition, it was found that when Ga is incorporated into CdTe it may induce anti-site defects of the type Cd_{Te}, leading to a compensating complex (Babentsov *et al.*, 2001). When observed locally, these configurations are expected to differ considerably in their atomic arrangements, as compared with the pure undistorted crystal.

The DX- and A-center complexes (Fig. 1) are important types of defects, often held responsible for limiting the doping efficiency in a broad range of semiconductors. While their existence in most cases is confirmed only indirectly, there are several experimental studies with more direct measurements.

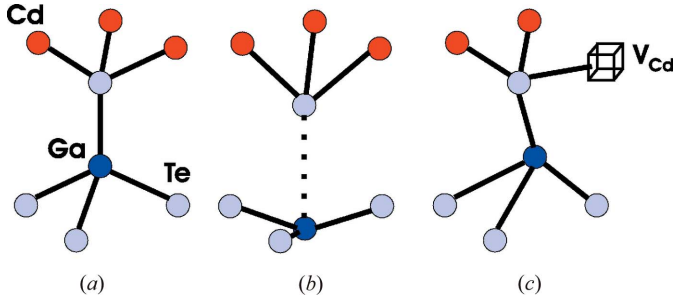

Figure 1
Sketch of the atomic structure of the Ga defects to be considered: (*a*) the substitutional position Ga(Cd), (*b*) Ga(Cd) DX-center and (*c*) Ga(Cd) A-center.

Cd vacancies associated with the A-center defects in CdTe have been confirmed by positron annihilation spectroscopy (Kauppinen *et al.*, 1997). Large lattice instability, accompanied by the shortening of one of the four Cd nearest-neighbor (NN) bond lengths, has been observed in the EXAFS signal of heavily indium-doped CdTe (Espinosa *et al.*, 1997). In another X-ray absorption study, the photoinduced lattice relaxation around indium is attributed to the presence of DX-centers, whereas the A-center defects are considered to be dominant types of defects at lower dopant concentration (Espinosa *et al.*, 2000). Other locally sensitive methods, such as perturbed angular correlations in combination with density functional theory (DFT) calculations (Lany *et al.*, 2004), have also been employed to gather information about CdTe:In on the local scale. Here, the assignment of the measured electric field gradient to the defect in question was possible due to DFT calculations.

With progress both in the experimental determination of local structures by X-ray absorption techniques and in theoretically modeling local structures with improved DFT calculations we are now able to report in this paper on a quite precise determination of the local structure around Ga in CdTe. EXAFS spectra were obtained on samples doped with Ga under conditions that would make it feasible to achieve high concentrations of DX- and A-center defects, so that the contribution of these defect configurations to the total EXAFS signal would be detectable. We show that the EXAFS spectra of the highly doped Ga samples cannot be successfully fitted by assuming only one substitutional Ga_{Cd} fraction. Instead, we demonstrate that the superposition of at least three different local configurations is needed for a satisfactory fit to the measured EXAFS data. Given that the absorption is measured at the Ga *K*-edge, the possible Cd on Te anti-site defects, induced by the incorporation of Ga in Cd_{Te}, are of little concern for this study. We will not be sensitive enough to clearly distinguish a contribution from such a complex, but it may well be an additional fraction. By performing all-electron DFT calculations, we were able to obtain an accurate theoretical description of the local coordinations of the different defect structures, and use it as the starting point in our fitting of the EXAFS data. Our results are also complemented by XANES model simulations, enabling an additional qualitative comparison with the experimental data.

2. Experimental and data processing

For our EXAFS data acquisition we prepared two types of samples: one, designated as S1, was prepared from the top of the CdTe⟨Ga⟩ ingot with a gallium concentration of $\sim 9 \times 10^{18}$ atoms cm^{-3} in the melt. The other sample, S2, was made from CdTe⟨Ga⟩ additionally saturated by Ga at 1123 K over 1.5 months. The estimated Ga concentration of the S2 sample is $\sim 10^{20}$ atoms cm^{-3}. This concentration is suitable for studying DX- and A-center defects. Samples with higher concentrations than, for example, $\sim 10^{21}$ atoms cm^{-3} might lead to additional defect structures, making the physical picture even more complicated.

The EXAFS measurements were performed at the A1 beamline of HASYLAB with the absorption spectra collected at 20 K, 80 K and room temperature. Absorption was measured at the Ga *K*-edge in fluorescence mode with a seven-segment Ge detector at 90° and in line with the polarization vector of the incoming synchrotron radiation. After background reduction and normalization, the EXAFS spectra $\chi(E)$ were transformed to *R*-space using the *IFFEFIT* package (Ravel & Newville, 2005).

Subsequent analysis and fitting was performed with Kaiser–Bessel windows with ramp width of 1.0 Å^{-1} from roughly 3.5 to 13 Å^{-1} for the S1 sample and 3.5 to 14 Å^{-1} for the S2 sample. The fitting procedure was carried out in *R*-space from 1.25 to 3.9 Å^{-1}.

3. *Ab initio* calculations

Our calculations were performed using the linear augmented plane waves plus local orbitals (LAPW+lo) method, as implemented in the *wien2k* (Blaha *et al.*, 2001) code. Starting from the optimized lattice parameter a = 6.63 Å of CdTe, we constructed a 2 × 2 × 2 supercell in body-centered cubic symmetry, wherein one Cd atom was replaced by Ga. This supercell was used to model the various charge states of the substitutional, DX- and A-center configuration in the presence of a uniform compensating background charge of opposite sign. The A-center defect was calculated after removing one metal atom from the next-nearest-neighbor (NNN) shell, whereas for the DX structures Ga was displaced along the $[\bar{1}, \bar{1}, \bar{1}]$ direction, breaking its point-group symmetry from T_d to C_{3v}. We relaxed all atoms in the supercell along the predefined symmetry directions with a force criterion of 3 mRy a.u.$^{-1}$ up to the third shell around Ga, the fourth shell being fixed to the lattice parameter owing to symmetry restrictions. Going to a larger 3 × 3 × 3 supercell would bring certain improvements regarding the accuracy of the calculated distances. It would also increase the number of shells that could be relaxed around Ga. However, this supercell would contain 216 atoms (38 non-equivalent) which would dramatically increase the computational overhead of the simulation. As far as our results are concerned, this improvement would not be crucial since the calculated distances are only used as starting values in the EXAFS fit. In addition, our fit includes paths only from within the first three shells of each of the calculated defect structures, so the relaxation of the more distant shells is not needed.

In the LAPW+lo calculations, the basis set functions were expanded up to $R_{mt}K_{max} = 7$, with R_{mt} being the smallest radius of the atomic muffin tin (MT) spheres, and K_{max} the magnitude of the largest reciprocal lattice vector in the basis of plane waves. The radii of the MT spheres for Cd, Te and Ga were set to 2.5, 2.5 and 2.3 a.u., respectively. The irreducible part of the Brillouin zone was sampled with 10 *k*-points. We used the generalized gradient approximation in the PBE parameterization (Perdew *et al.*, 1996). The charge difference of 0.00001 electrons between two consecutive iterations was chosen as the convergence criterion.

For our simulations of the XANES spectra we used the *ab initio* multiple-scattering *FEFF*8 program (Ankudinov *et al.*, 1998). *FEFF*8 is capable of performing full-multiple-scattering (FMS) calculations to improve the modeling of the near-edge region. Simulations were conducted on a cluster of roughly 200 atoms. The atoms in the vicinity of the absorbing atom (within a sphere of ~11.5 Å) were arranged according to the calculated lattice relaxation, as obtained from our LAPW+lo calculations. The remaining atoms were fixed to their undistorted lattice positions. The potential was calculated self-consistently (SCF card), and the FMS mode was turned on. Additionally, we introduced 0.5 eV broadening to account for the experimental resolution. Also, we improved the interstitial density of this relatively open system by using the INTERSTITIAL card. Putting extra charge on the central atom to account for the different charge states of the defect systems was found to have no practical effect on the calculated spectra, as the charge transfer between the neighboring atoms is obviously already taken care of with the use of the SCF capabilities of *FEFF*8.

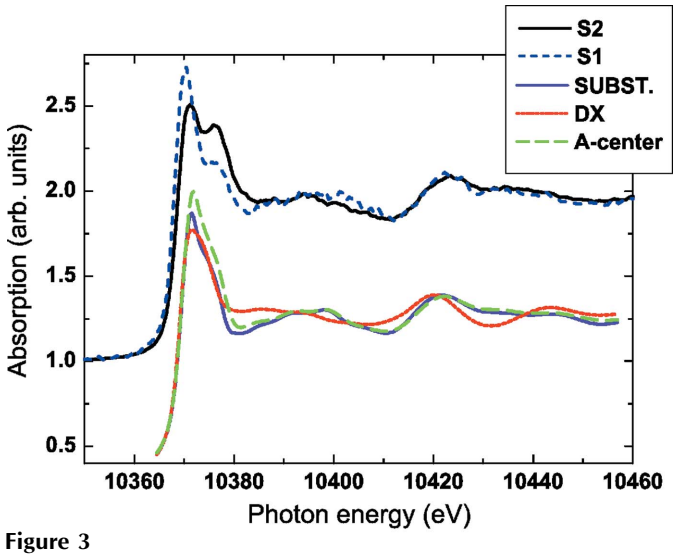

Figure 3
Comparison of the experimental near-edge EXAFS S1 and S2 spectra (top) with spectra calculated for different configurations around Ga in CdTe (bottom): Ga substitutionally incorporated in Cd (full line), Ga in the DX configuration (short dashed line), and Ga in an A-center environment (long dashed line). The theoretical spectra are normalized to the height of the experimental edge step and shifted in the *y*-direction for easier comparison.

4. Results and discussion

The upper panel of Fig. 2 depicts the Fourier transform (FT) of the *k*-weighted experimental EXAFS spectra $\chi(k)$. Qualitatively, in the heavily doped S2 sample we observe a decrease in magnitude of the most dominant peak with respect to the sample with lower Ga concentration. This peak is associated with the first-shell environment around the dopant and, in principle, all different Ga local arrangements contribute to its intensity. The distinctive shoulder that appears in the region from 2.7 to 3 Å is more pronounced in the S2 EXAFS, indicating that the addition of Ga strongly modifies the local environment in CdTe, and that contributions other than the substitutional are becoming visible in the EXAFS signal.

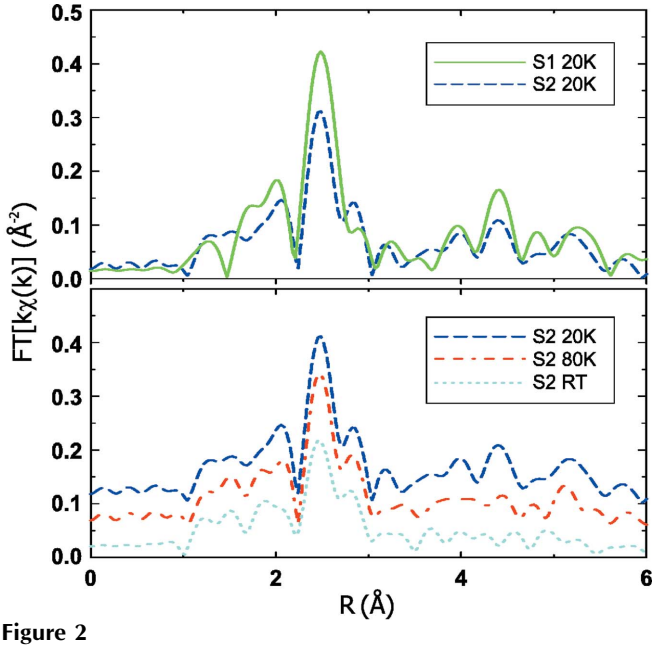

Figure 2
Radial distribution functions of Ga in CdTe obtained from the EXAFS spectra, weighted linearly with *k* and Fourier transformed.

Fig. 2 (lower part) depicts the temperature dependence of the EXAFS data collected on the S2 sample. The decrease in amplitude in this case is due to the temperature-dependent Debye–Waller factors, and qualitative inspection shows that there are no indications of possible structural rearrangements of the local atomic coordinations with temperature. Furthermore, the positions of the main peaks seem to be temperature-independent, indicating that there are virtually no changes in the nearest bond lengths within the investigated temperature range.

The experimental XANES spectra, along with our model XANES simulations, are shown in Fig. 3. The experimental S1 and S2 XANES curves, while matching each other relatively well beyond 10385 eV, exhibit some pronounced differences immediately at and above the edge step. In particular, the S2 sample shows a decrease in the white-line intensity accompanied with an increase in the intensity of the nearest shoulder located at 10376 eV. Our model calculations for the substitutional and A-center positions also predict an intense white line, more dominant in the latter case. The simulated XANES for the DX-center configuration, however, exhibits a reduction in white-line intensity, which is a hint that the observed white-line intensity change of the S2 XANES could be associated with this type of defect. The only feature that our model computations completely fail to describe is the presence and behavior of the shoulder nearest to the white line.

While we were able to successfully fit the S1 EXAFS spectrum by including only the substitutional model configuration [with the fitted NN distance of 2.64 (1) Å, and σ^2 = 0.0023 (7) Å^2], the satisfactory fit of the S2 EXAFS spectrum required additional contributions (Fig. 4). For the heavily

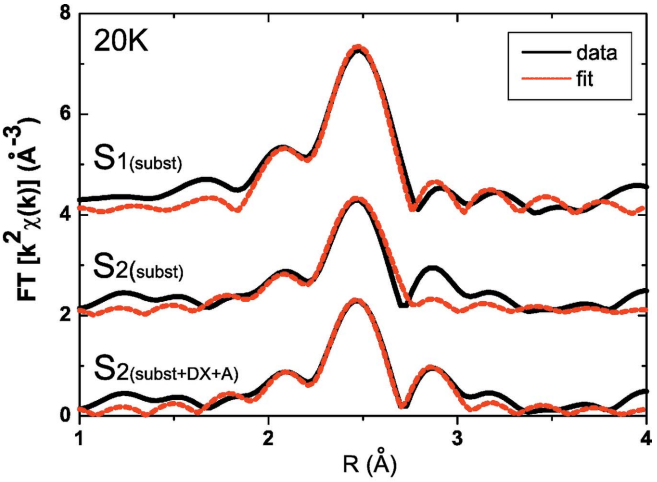

Figure 4
Radial distribution functions of the S1 EXAFS spectrum fitted with the substitutional Ga contribution (top). The same fitting model was not successful in the case of the S2 EXAFS (center), where all three local configurations were required in order to produce a satisfactory fit (bottom).

doped sample, the starting basis of our fitting model was deduced by qualitative comparison of the experimental S2 EXAFS with the superposition of the theoretical FEFF path standards (see Fig. 5) for each of the three different local environments around Ga [according to the *wien2k* calculated fully relaxed structures (see below)].

The sums of the most important theoretical scattering paths (up to a distance of 4.5 Å from the absorbing atom) for the DX-center, $Ga(Cd)_{DX}$, A-center, $Ga(Cd)_{A}$, and substitutional, $Ga(Cd)_{subst}$, local environments are presented in Fig. 5. They were obtained by running *FEFF*8 on a cluster of atoms in real space arranged according to the lattice relaxation calculated by *wien2k*. The amplitude reduction factor, S_0^2, for each path in the sum was set to 0.9, the energy shift, E_0, to 0, whereas the

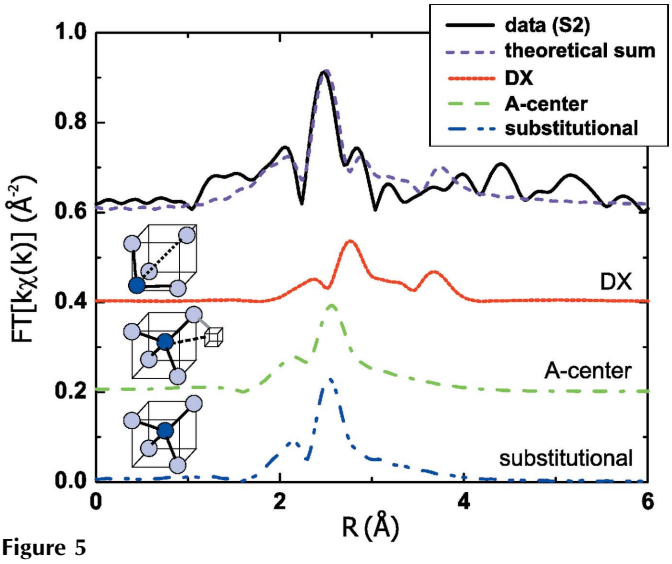

Figure 5
DX-center, A-center and substitutional contributions to the theoretical EXAFS sum calculated by *FEFF*8 compared with the S2 EXAFS data collected at 20 K.

Table 1
Calculated LAPW distances for the different Ga(Cd) configurations.

	Bond	Distance (Å)	Coordination number
$Ga(Cd)^{1+}_{subst}$	Ga—Te	2.72	4 (Te)
	Ga—Cd	4.69	12 (Cd)
$Ga(Cd)^{1-}_{DX}$	Ga—Te	2.95	3 (Te)
	Ga—Te	3.61	1 (Te)
	Ga—Cd	3.95	3 (Cd)
	Ga—Te	4.66	3 (Te)
	Ga—Te	4.84	6 (Cd)
$Ga(Cd)^{1-}_{A\text{-center}}$	Ga—Te	2.66	1 (Te)
	Ga—Te	2.73	1 (Te)
	Ga—Te	2.75	2 (Te)
	Ga—Cd	4.55–4.75	11 (Cd)

mean-squared displacements, σ^2, were set to the values obtained from the Debye model.

Both $Ga(Cd)_{subst}$ and $Ga(Cd)_{A}$ environments contribute to the main peak; the former is more pronounced owing to the single fourfold coordinated Te NN shell. The first shell of the $Ga(Cd)_{A}$ configuration is distorted and thus the resulting EXAFS signal is smeared out. The Ga central atom in the $Ga(Cd)_{DX}$ configuration is moved away from the threefold-coordinated Te NN shell and therefore the contribution from this shell is dominant farther to the right, in the region of the right-hand shoulder of the main peak. These three configurations, with fixed bond lengths according to our LAPW calculations (Table 1), were then given equal weighting, added together, and the amplitude of the total sum was adjusted to match those of the experimental spectrum.

We see that in the EXAFS of the heavily doped Ga sample there are at least three local contributions, and the theoretical EXAFS sum of these configurations (the distances were not allowed to vary from their computed values), even without fitting, matches the experimental data very well (Fig. 5). One has to bear in mind that the non-*ab-initio* σ^2 parameters obtained from the Debye model are not accurate, and that the relative ratio of the FT magnitude of the individual paths can change, as they indeed do in the actual fit (Fig. 4).

Our calculations predict a sizeable bond-length contraction (2.72 Å) for the positively charged substitutional $Ga(Cd)_{subst}$ position. The undisturbed CdTe bond length is 2.81 Å. As expected, the charge of the defect strongly influences the relaxation, which is reflected in the calculated neutral $Ga(Cd)_{subst}$ NN distance of 2.83 Å. The NN distances of the negatively charged $Ga(Cd)_{A}$ state are distributed in several subshells close to the bond length obtained for the substitutional position. Our calculations indicate that the lattice relaxation of the $Ga(Cd)_{DX}$ position is also quite large. After bond breaking, a stable position of the impurity is found 0.99 Å from the original position in the $[\bar{1}\bar{1}\bar{1}]$ antibonding direction. The [111] Te atom is also displaced in the same direction by 0.23 Å. The net effect is that the state has a markedly different local relaxation, with NN distances expanded by more than 0.2 Å compared with the substitutional position.

Given that the EXAFS data were obtained at three different temperatures, we arranged a multiple data set fitting that allowed us to effectively limit the number of variables and

Table 2
EXAFS parameters as obtained from the multiple datasets' fitting of the heavily doped Ga in the CdTe (S2) sample (RT = room temperature).

Bond	Fraction (%)	R (Å)	N	σ^2 (Å^2)
$Ga(Cd)_{subst}$				
Ga—Te	0.45	2.66 (4)	4	0.0017 (2), 20 K 0.002 (2), 80 K 0.003 (4), RT
$Ga(Cd)_{DX}$				
Ga—Te	0.25	3.10 (2)	3	0.0015 (1), 20 K 0.002 (2), 80 K 0.001 (3), RT
Ga—Cd	0.25	3.71 (4)	3	0.004 (4), 20 K 0.02 (4), 80 K 0.01 (1), RT
$Ga(Cd)_{A}$				
Ga—Te	0.30	2.56 (13)	1	0.0015 (5), 20 K 0.002 (5), 80 K 0.01 (1), RT
Ga—Te	0.30	2.92 (29)	3	0.01 (1), 20 K 0.02 (1), 80 K 0.01 (1), RT

their correlations and to improve the quality of the fit. In order to avoid the numerous contributions from the scattering paths in the region around 4.5 Å, the fitting range in R-space was from 1.25 to 3.9 Å. Owing to the fact that the bond lengths are virtually temperature-independent within the measured range, the mutual parameters across the temperature data sets were the bond lengths for each of the paths, their corresponding ΔE_0 parameters, as well as the ratio of the fractions. Owing to the different electronic structure around the impurity atom in the three contributions considered here, it is more favorable to assign a different ΔE_0 to each fraction, instead of a single ΔE_0 for the whole data set. The data sets were fitted with separate amplitude reduction factors, S_0^2, also leaving the σ^2 parameters for each path as free variables. In order to further reduce the number of free parameters, some of the paths with lesser importance were excluded from the fit (see Table 2). In total, we used 27 variables to fit our data sets for the S2 sample. Because our fitting procedure was based on simultaneously fitting three data sets with 35 independent data points (Nyquist Formula) we had enough degrees of freedom to accommodate this high number of free parameters. This fitting model, although somewhat rigid, was chosen in order to describe the physics of the system without introducing too many variables and keeping their correlations as low as possible. This strategy is supported by the quality of the fit ($R_{\rm factor}$ in *FEFFIT*) which came out within the limits of a good fit, comparable with the fit of the low-concentration CdTe⟨Ga⟩ sample (S1) with the substitutional configuration only. The results of the fit are summarized in Table 2.

As can be seen, the best fit was found for 45% of Ga atoms occupying the substitutional, 25% the DX-center and 30% the A-center configuration. These figures for the fractions would presumably change if a fourth fraction was allowed for a possible Ga complex formed with a Cd anti-site. All the fitted distances agree reasonably well with our calculated bond lengths. In particular, the NN Ga—Te bond length for the substitutional Ga position of 2.66 (4) Å is in relatively good agreement with our calculated value of 2.72 Å. As expected, it also agrees well with the corresponding value obtained for the S1 sample. Our fitted DX distances are larger by up to 0.15 Å compared with the calculated values, a discrepancy which is probably due to the limited supercell size.

The evidence presented for the formation of A- and DX-centers when Ga is introduced into CdTe resembles the situation with Br in CdTe (Mahnke *et al.*, 2004, 2005). For Br in CdTe, careful analysis of the EXAFS spectra revealed the occurrence of both A-centers and most likely DX-centers as well. However, for Br no reference sample was observed with only substitutional Br, although the concentration was comparable with the Ga in the CdTe sample S1 in our investigation. This was interpreted as resulting from the slight lattice expansion around a substitutional Br acting as the driving force for the formation of A- and DX-centers. In the present case of Ga in CdTe, the relaxation around Ga facilitates the substitutional incorporation leading to additional A- and DX-centers only at higher concentrations.

5. Conclusion

Relying on the theoretically predicted local configurations, the most likely reason for the decrease in EXAFS amplitude of the heavily Ga-doped sample is the appearance of additional A-center and DX-center contributions, resulting in a less sharply defined fourfold neighborhood and a distorted NN shell. The shoulder around 3 Å has been traced down to EXAFS contributions from local configurations which have undergone a deep relaxation, *i.e.* DX-configurations. Our EXAFS analysis has been able to account for these configurations and for the first time directly extract the local structural parameters.

Our results indicate that the measured absorption spectra on the heavily doped CdTe:Ga sample cannot be explained using only one substitutional donor configuration, whereas the inclusion of additional DX- and A-center local environments considerably improves the fits. The additional indication of the validity of this model is the good agreement between the fitted and calculated bond lengths.

VK and JBC would like to acknowledge the help of the Serbian Ministry of Science and Education, under Grant No. ON171001. This work was largely supported by the former Hahn–Meitner-Institut, now the Helmholtz–Zentrum Berlin für Materialien und Energie GmbH, when VK as a visiting scientist and H-EM as a senior scientist were members of the institute. Finally the authors gratefully acknowledge the hospitality and help they experienced at HASYLAB at DESY, especially from E. Welter.

References

Ankudinov, A. L., Ravel, B., Rehr, J. J. & Conradson, S. D. (1998). *Phys. Rev. B*, **58**, 7565–7576.
Babentsov, V., Corregidor, V., Castaño, J. L., Fiederle, M., Feltgen, T., Benz, K. W. & Diéguez, E. (2001). *Cryst. Res. Technol.* **36**, 535.

Blaha, P., Schwarz, K., Madsen, G., Kvasnicka, D. & Luitz, J. (2001). *Wien2k, An Augmented Plane Wave + Local Orbitals Program for Calculating Crystal Properties*. K. Schwarz, Technische Universität Wien, Austria.
Chadi, D. J. & Chang, K. J. (1988). *Phys. Rev. Lett.* **61**, 873–876.
Del Sordo, S., Abbene, L., Caroli, E., Mancini, A. M., Zappettini, A. & Ubertini, P. (2009). *Sensors*, **9**, 3491.
Espinosa, F. J., de Leon, J. M., Conradson, S. D., Peña, J. L. & Zapata-Torres, M. (2000). *Phys. Rev. B*, **61**, 7428–7432.
Espinosa, F. J., Mustre de Leon, J., Zapata-Torres, M., Castro-Rodriguez, R., Peña, J. L., Conradson, S. D. & Hess, N. J. (1997). *Phys. Rev. B*, **55**, 7629–7632.
Fochuk, P., Korovyanko, A., Turkevich, I. & Panchuk, O. (2002). *Inorg. Mater.* **38**, 350–354.
Fochuk, P., Panchuk, O. & Korovyanko, O. (2004). *J. Alloys Compd.* **371**, 10–14.
Kauppinen, H., Baroux, L., Saarinen, K., Corbel, C. & Hautojärvi, P. (1997). *J. Phys. Condens. Matter*, **9**, 5495.
Koteski, V., Haas, H., Holub-Krappe, E., Ivanovic, N. & Mahnke, H.-E. (2005). *Phys. Scr.* T**115**, 369.
Lany, S., Wolf, H. & Wichert, T. (2004). *Phys. Rev. Lett.* **92**, 225504.
Mahnke, H.-E., Haas, H., Holub-Krappe, E., Koteski, V., Novakovic, N., Fochuk, P. & Panchuk, O. (2005). *Thin Solid Films*, **480–481**, 279–282.
Mahnke, H.-E., Haas, H., Koteski, V., Novakovic, N., Fochuk, P. & Panchuk, O. (2004). *Hyperfine Interact.* **158**, 353–359.
Panchuk, O. & Fochuk, P. (2010). *CdTe and Related Compounds; Physics, Defects, Heteroand Nano-structures, Crystal Growth, Surfaces and Applications*, edited by R. Triboulet and P. Siffert, pp. 309–362. Amsterdam: Elsevier.
Park, C. H. & Chadi, D. J. (1995). *Phys. Rev. B*, **52**, 11884–11890.
Perdew, J. P., Burke, K. & Ernzerhof, M. (1996). *Phys. Rev. Lett.* **77**, 3865–3868.
Ravel, B. & Newville, M. (2005). *J. Synchrotron Rad.* **12**, 537–541.
Triboulet, R. & Siffert, P. (2010). Editors. *CdTe and Related Compounds; Physics, Defects, Hetero- and Nano-structures, Crystal Growth, Surfaces and Applications.* Amsterdam: Elsevier.
Rössler, U. (1999). Editor. *Landolt-Börnstein, Numerical Data and Functional Relationships in Science and Technology, Group III: Condensed Matter*, Suppl. to III/17*b*, 22a, Vol. 41. Berlin, Heidelberg: Springer.